JOURNAL OF APPLIED ELECTROCHEMISTRY **29**: 171–176, 1999.


# Modelling of phosphoric acid fuel cell cathode behaviour

G. MAGGIO

*CNR Institute for Transformation and Storage of Energy, Salita S.Lucia sopra Contesse 5, 98126 S. Lucia, Messina, Italy (e-mail: itae@itae.me.cnr.it)*

Received 23 September 1997; accepted in revised form 6 July 1998

A mathematical model for phosphoric acid fuel cell (PAFC) cathodes has been developed. The model, based on equations that take activation and diffusional problems into account, provides a description of the electrochemical behaviour of the electrode. These studies allow optimization of the morphological characteristics of this cell component and improvement in the performance of the whole fuel cell. In particular, the sensitivity analysis carried out on the model provides information on the influence of single parameters. Accordingly, the as optimized cathode allowed a performance of 700 mV at 200 mA $cm^{-2}$ in air; the corresponding cell potential also increased from 500 mV at 150 mA $cm^{-2}$ to 510 mV at 200 mA $cm^{-2}$.

Keywords: *cathodic polarization*, *cell potential*, *modelling*, *optimization*, *phosphoric acid fuel cells*

**List of symbols**

| | |
|---|---|
| $C$ | oxygen concentration (mol $cm^{-3}$) |
| $C_0$ | gas-phase oxygen concentration (mol $cm^{-3}$) |
| $D$ | gaseous diffusion coefficient in the agglomerates ($cm^2\ s^{-1}$) |
| $F$ | Faraday constant (96 487 C $mol^{-1}$) |
| $i$ | current density (A $cm^{-2}$) |
| $\bar{i}$ | average current density on the agglomerate (A $cm^{-2}$) |
| $i_0$ | exchange current density (A $cm^{-2}$) |
| $j$ | total current density produced by the electrode (A $cm^{-2}$) |
| $j_0$ | effective exchange current density of the porous electrode (A $cm^{-2}$) |
| $n$ | number of electrons transferred in the electrochemical reaction (g equiv. $mol^{-1}$) |
| $PAO$ | percentage of acid occupation (Equation 25) |
| $R$ | gas constant (8.314 J $mol^{-1}K^{-1}$) |
| $Ra$ | average agglomerate radius (cm) |
| $r$ | radial coordinate (cm) |
| $s$ | empirical exponent used as porosity–tortuosity factor of the agglomerates |
| $T$ | absolute temperature (K) |
| $z_c$ | catalyst layer thickness (cm) |

*Greek symbols*

| | |
|---|---|
| $\alpha_c$ | cathodic transfer coefficient |
| $\eta$ | cathodic overpotential (V) |
| $\eta_T$ | Tafel slope (V) |
| $v$ | active surface area of catalyst per volume of catalyst layer ($cm^2\ cm^{-3}$) |
| $v'$ | surface area of catalyst per volume of agglomerate ($cm^2\ cm^{-3}$) |
| $\theta$ | average agglomerate porosity |
| $\rho$ | diffusive modulus (Equation 15) |

## 1. Introduction

Several mathematical models devoted to the optimization of fuel cell components, are reported in the literature, for example [1–7]. This paper deals with a model for the performance evaluation of Teflon®-bonded porous electrodes for oxygen or air reduction in phosphoric acid (PAFC cathode). The model, based on coupled analysis of gaseous diffusion and reaction kinetic mechanisms, correlates the morphological characteristics of the electrode to its electrochemical behaviour, and gives voltage values corresponding to prefixed current densities (IV curves).

A fuel cell electrode consists of a diffusional layer, constituted by a porous support made of partially hydrophobic carbon-paper, and a catalytic layer. This latter can be viewed as composed of regions containing platinum, carbon and Teflon® (Pt–C–PTFE), in which the microporosity (pores with diameter lower than 2 nm [8]) is localized. These regions are crossed by macropores (>50 nm [8]) accessible to gas flow. The Pt–C–PTFE regions form the so-called agglomerates that can be more or less wetted by the electrolyte, that is, phosphoric acid (Fig. 1). Teflon®, acts as binding agent and determines the hydrophilic–hydrophobic properties of the electrode. The active surface area of the catalyst is related to the portions of gas and electrolyte in the catalyst layer, the active sites for the electrochemical reaction being those where a three-phase gas/electrolyte/catalyst contact is established.

The model assumes that the agglomerates have a spherical geometry, with prefixed size and porosity, and is characterized by a basic equation including as limiting cases both activation and diffusion control.

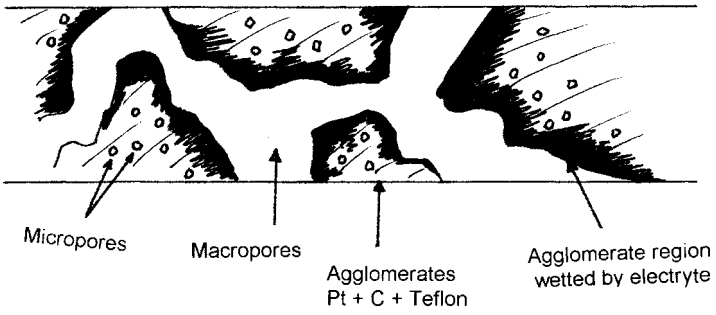


Fig. 1. Schematic representation of the catalyst layer structure.

## 2. Model equations

The electrochemical reaction occurring at the cathode of a PAFC is

$$1/2\ O_2 + 2\ H^+ + 2\ e^- \rightarrow H_2O$$

The reaction-diffusion equation [9] is

$$nFD\theta^s \frac{1}{r}\frac{d^2(rC)}{dr^2} = v'i \tag{1}$$

where the current density $i$ and the oxygen concentration $C$ are a function of the radial coordinate $r$ along the agglomerate.

By assuming a first order reaction for the gaseous reactant that controls the diffusive process (oxygen), equation (1) can be written as

$$nFD\theta^s \frac{1}{r}\frac{d^2(rC)}{dr^2} = v'i_0 \frac{C}{C_0}\exp(\alpha_c F\eta/RT) \tag{2}$$

This differential equation must be solved with the boundary conditions

$$C = C_0 \quad \text{at} \quad r = Ra \tag{3}$$

and

$$dC/dr = 0 \quad \text{at} \quad r = 0 \tag{4}$$

which establish, respectively, that the oxygen concentration on the agglomerate surface is equal to its equilibrium (gas phase) value and that there is no diffusive flow through the centre of the agglomerate, as required by symmetry. The concentration profiles along the agglomerate are depicted in Fig. 2, where the case of an electrolyte film covering the agglomerate, for excess acid, is also presented (Fig. 2(b)).

The average current density on the agglomerate can be calculated as

$$\bar{i} = \frac{\int_0^{Ra} ir^2 dr}{\int_0^{Ra} r^2 dr} = \frac{3\int_0^{Ra} ir^2 dr}{Ra^3} \tag{5}$$

To solve the integral at the numerator of Equation 5, the explicit expression for current density from Equation 1 can be utilized:

$$\int_0^{Ra} ir^2 dr = \frac{nFD\theta^s}{v'}\int_0^{Ra}\frac{d^2(rC)}{dr^2} r dr$$

$$= \frac{nFD\theta^s}{v'} Ra^2 \left.\frac{dC}{dr}\right|_{r=Ra} \tag{6}$$

Then, the average current density on the agglomerate becomes

$$\bar{i} = \frac{3nFD\theta^s}{v'Ra}\left.\frac{dC}{dr}\right|_{r=Ra} \tag{7}$$

where the derivative of the concentration must be calculated.

Now, by considering Equation 2, we have

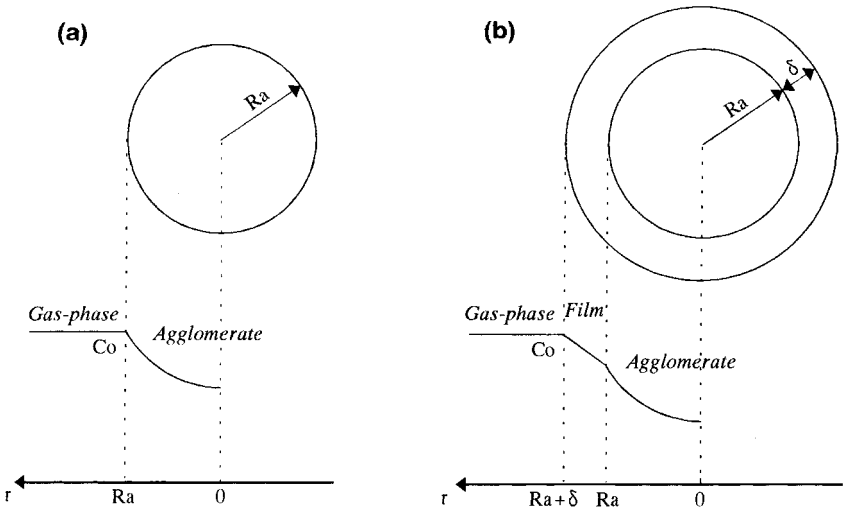


Fig. 2. Oxygen concentration profiles for the 'dry' agglomerate (a) and for the agglomerate covered by an electrolyte film of thickness $\delta$ (b).

$$\frac{d^2(rC)}{dr^2} - \frac{v' i_0 \exp(\alpha_c F\eta/RT)}{nFDC_0\theta^s} rC = 0 \quad (8)$$

that is a second order ordinary differential equation at constant coefficients.

Integration of this equation results in

$$C = \frac{k_1 e^{\sqrt{k}r} + k_2 e^{-\sqrt{k}r}}{r} \quad (9)$$

with $k_1$ and $k_2$ arbitrary constants, that can be specified by applying the boundary conditions 3 and 4; and

$$k = \frac{v' i_0 \exp(\alpha_c F\eta/RT)}{nFDC_0\theta^s} \quad (10)$$

Thus, the derivative of Equation 9 is

$$\frac{dC}{dr} = \frac{\left(k_1\sqrt{k}e^{\sqrt{k}r} - k_2\sqrt{k}e^{-\sqrt{k}r}\right)r - \left(k_1 e^{\sqrt{k}r} + k_2 e^{-\sqrt{k}r}\right)}{r^2} \quad (11)$$

It can be easily verified that the boundary condition 4 provides $k_1 + k_2 = 0$ (i.e., $k_2 = -k_1$); from the boundary condition 3 we obtain

$$C_0 = \frac{k_1 e^{\sqrt{k}Ra} + k_2 e^{-\sqrt{k}Ra}}{Ra} \quad (12)$$

and then

$$k_1 = \frac{Ra\ C_0}{e^{\sqrt{k}Ra} - e^{-\sqrt{k}Ra}} \quad (13)$$

Therefore, the derivative of the concentration, calculated at $r = Ra$, becomes

$$\left.\frac{dC}{dr}\right|_{r=Ra} = \frac{C_0}{Ra}\left[\sqrt{k}Ra\coth\left(\sqrt{k}Ra\right) - 1\right] = \frac{C_0}{Ra}\left[\rho\coth(\rho) - 1\right] = \frac{C_0\rho}{Ra}\mathscr{L}(\rho) \quad (14)$$

where

$$\rho = \sqrt{k}Ra = \left(\frac{v' i_0 Ra^2}{nFDC_0\theta^s}\right)^{1/2} \exp(\alpha_c F\eta/2RT) \quad (15)$$

represents a diffusive modulus whose meaning will be clarified below, and

$$\mathscr{L}(\rho) = \coth(\rho) - \rho^{-1} \quad (16)$$

is the Langevin function.

By substituting Equation 14 in Equation 7 for the average current density is

$$\bar{i} = \frac{3nFDC_0\theta^s}{v'Ra^2}\rho\mathscr{L}(\rho) = 3i_0\left(\frac{v' i_0 Ra^2}{nFDC_0\theta^s}\right)^{-1}\rho\mathscr{L}(\rho) \quad (17)$$

and by invoking the expression of $\rho$ (Equation 15), we obtain

$$\bar{i} = 3i_0\rho^{-1}\exp(\alpha_c F\eta/RT)\mathscr{L}(\rho) \quad (18)$$

When the limitations on the ionic and electronic contributions to electrode conductivity are absent, the total current density produced by the electrode can be obtained by the product of the average current density on the agglomerate and the active (i.e., wetted by the electrolyte) Pt surface area:

$$j = \bar{i}vz_c = 3vi_0z_c\rho^{-1}\exp(\alpha_c F\eta/RT)\mathscr{L}(\rho) = 3j_0\rho^{-1}\exp(\eta/\eta_T)\mathscr{L}(\rho) \quad (19)$$

where $j_0 = vi_0z_c$ is the effective exchange current density of the porous electrode and $\eta_T = RT/\alpha_c F$ the Tafel slope.

The diffusive modulus, $\rho$, which appears in Equation 15, determines the conditions of activation and diffusion control of the electrode. In fact, according to the properties of the Langevin function

$$\mathscr{L}(\rho) \approx \begin{cases} \rho/3 & \text{for} \quad \rho \ll 1 \\ 1 & \text{for} \quad \rho \gg 1 \end{cases} \quad (20)$$

two limiting cases can be distinguished:
(i) for $\rho \ll 1$ Equation 19 becomes

$$j = j_0\exp(\eta/\eta_T) \quad (21)$$

that is,

$$\ln j = \ln j_0 + \eta/\eta_T \quad (22)$$

(ii) for $\rho \gg 1$ we obtain

$$j = \sigma j_0\exp(\eta/2\eta_T) \text{ with } \sigma = 3\left(\frac{nFDC_0\theta^s}{v' i_0 Ra^2}\right)^{1/2} \quad (23)$$

that is

$$\ln\ j = \ln(\sigma j_0) + \eta/2\eta_T \quad (24)$$

## 3. Results and discussion

Equations 22 and 24 allow discrimination between low and high current density regions, controlled by activation and diffusion, respectively, and characterized by a single ($\eta_T$) and a double Tafel slope ($2\eta_T$). This variation in the Tafel slope is also confirmed by literature data. Kunz and Gruver [10], in fact, considered a Tafel slope equal to about 90 mV decade$^{-1}$ in oxygen for a Teflon®-bonded cathode at 160 °C in 96% $H_3PO_4$ and a slope of 180 mV decade$^{-1}$ when the resistance to the oxygen diffusion becomes significant.

As shown in Fig. 3, the agreement between the theoretical polarization curves (model) and the experimental ones is very satisfactory (differences are less than 20 mV).

The model provides useful information on the influence of several parameters, including Teflon® amount in the catalyst layer, catalyst (Pt) loading and surface area, agglomerate porosity and radius, thickness of diffusional and catalyst layer etc., on the cathodic potential. The results of this sensitivity analysis are summarized in Table 1.

Figures 4–6 show the influence of catalyst layer thickness, weight percentage of Pt and Pt loading in the catalyst layer on the cathodic overpotential in air, calculated by varying the studied parameter and imposing for the others fixed values corresponding to a base-case reported in Table 2.

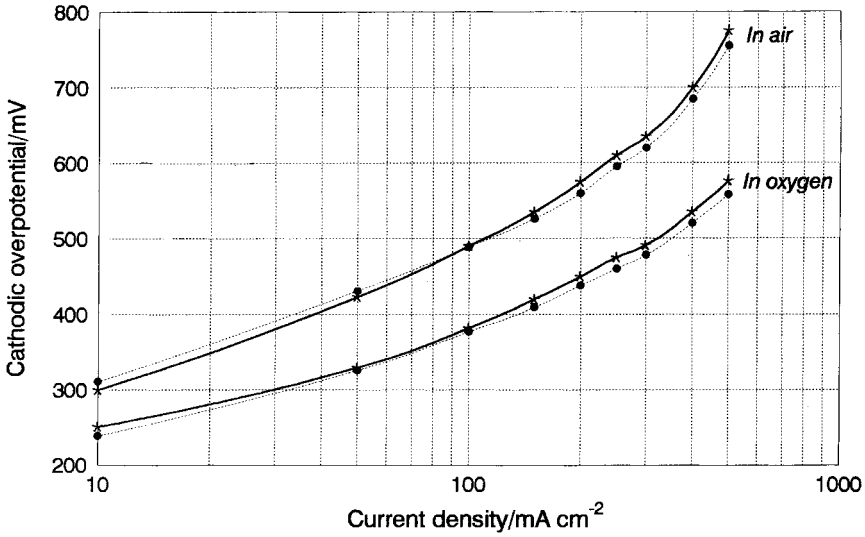


Fig. 3. Comparison between theoretical (model) (●) and experimental (∗) polarization curves. $T = 170\,^{\circ}C$; $P = 1$ atm; 0.5 mg Pt cm$^{-2}$; 40 wt % Teflon®; 10 wt % Pt/C.

*Table 1. Sensitivity analysis carried out on the main model parameters*

| *Parameter* | *Range of variation* | *Influence on the cathodic potential* | *Degree of influence* |
|---|---|---|---|
| Electrolyte ionic conductivity | 0.4–0.7 $\Omega^{-1}$ cm$^{-1}$ | Increases | Low (<25 mV). Higher at very high c.d. (>300 mA cm$^{-2}$) |
| Exchange c.d. | $10^{-6}$–$10^{-3}$ mA cm$^{-2}$ | Increases | High (~280 mV). Constant when c.d. changes |
| Oxygen solubility–diffusivity product | $6.3 \times 10^{-14}$–$6.3 \times 10^{-10}$ mol cm$^{-1}$ s$^{-1}$ | Increases | High (until 200 mV). Increases when c.d. increases |
| Average agglomerate pore radius | 10–100 $\mu$m | Decreases | High (~170 mV). Almost constant when c.d. changes |
| Average agglomerate porosity | 30–90% | Increases | High (~150 mV). Almost constant when c.d. changes |
| Catalyst utilization | 30–100% | Increases | Mean (~50 mV). Almost constant when c.d. changes |
| Catalyst layer thickness | 50–500 $\mu$m | Decreases | Mean (<70 mV). Higher at high c.d. (>100 mA cm$^{-2}$) |
| Fraction of Teflon® in the catalyst layer | 20–60% | Decreases | Low (<30 mV). Negligible at low c.d. (<200 mA cm$^{-2}$) |
| Fraction of Pt in the catalyst layer | 10–80% | Shows a 'bell-shaped' behaviour with a max at around 50% of Pt | Mean (< 60 mV). For values higher than 50% its influence is more marked at high c.d. (>100 mA cm$^{-2}$) |
| Percentage of acid in the catalyst layer | 20–70% | Shows a 'bell-shaped' behaviour with a max at around 50% of *PAO* | High (until 150 mV). Increases when c.d. increases |
| Pt loading in the catalyst layer | 0.25–1 mg cm$^{-2}$ | Increases | High (~130 mV). Almost constant when c.d. changes |
| Catalyst surface area | 50–80 m$^2$ g$^{-1}$ | Increases | Low (~20 mV). Constant when c.d. changes |
| Diffusional layer thickness | 0.004–0.4 cm | Decreases | Mean (<50 mV). Higher at high c.d. (>100 mA cm$^{-2}$) |
| Diffusional layer porosity | 10–80% | Increases | Mean (until 100 mV). Higher at high c.d. (>100 mA cm$^{-2}$) |

Note: c.d. = current density.

Details on the correlation between the parameters of the mathematical model and the experimental data can be found in [11].

The correlation between the morphological characteristics of the electrode and its electrochemical activity suggested modification of the preparation of the cathodes. Accordingly, with a Pt loading of 0.5 mg cm$^{-2}$, 20% of Pt/C and 40% of Teflon® in the catalyst layer, the measured performance was almost 700 mV at 200 mA cm$^{-2}$ (air, $T = 170\,^{\circ}C$, 98% $H_3PO_4$). This value compares favourably with state-of-the-art electrodes [12, 13].

The potential losses associated with cathodic polarization greatly affect the performance of a fuel cell, with a contribution in the order of 90% on the total polarizations at a current density of 200 mA cm$^{-2}$

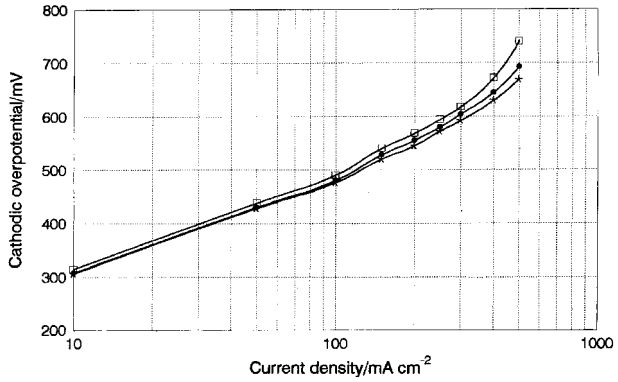


Fig. 4. Influence of the catalyst layer thickness on model results. Thickness: (∗) 50, (●) 200 and (□) 500 μm. Conditions: as given in Fig. 3.

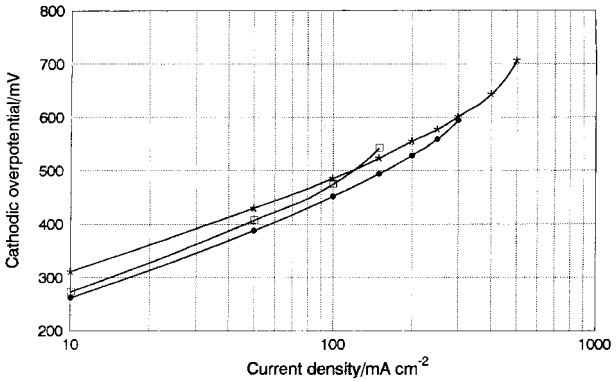


Fig. 5. Influence of the fraction of platinum in the catalyst layer on model results. Fraction: (∗) 10%, (●) 50% and (□) 80%. Conditions: $T = 170\,^{\circ}C$; $P = 1$ atm; 0.5 mg Pt $cm^{-2}$; 40 wt % Teflon®.

[14]. Therefore, this model has allowed, not only the understanding of the phenomena governing the behaviour of the single electrode, but also a considerable improvement in the experimental performance of the cell; passing from 500 mV at 150 mA $cm^{-2}$ (cell with a standard cathode) to 510 mV at 200 mA $cm^{-2}$.

This model also allowed a qualitative explanation of the 'bell-shaped' behaviour of the cathodic potential as a function of the percentage of acid that occupies the catalyst layer ($PAO$), defined as

$$PAO = \frac{\text{Volume of } H_3PO_4 \text{ absorbed in 24 h}}{\text{Pore volume of the catalyst layer}} \times 100 \quad (25)$$

Accordingly, two competitive effects associated with an increase of the $PAO$ must be taken into account, namely: (i) a decrease in the activation losses due to an increase in the available Pt area wetted by the electrolyte, and (ii) an increase in the diffusional losses caused by a thickening of the electrolyte film covering the agglomerates (this usually occurs when excess acid is present in the catalyst layer). Both contributions result in a performance maximum centred in the PAO range 40–60% (Fig. 7).

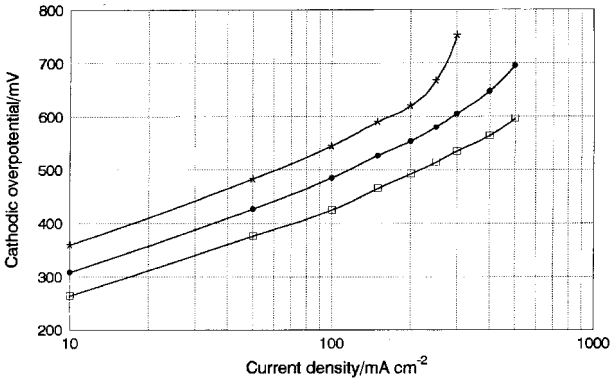


Fig. 6. Influence of the platinum loading in the catalyst layer on model results. Loading: (∗) 0.25, (●) 0.50 and (□) 1 mg $cm^{-2}$. Conditions: $T = 170\,^{\circ}C$; $P = 1$ atm; 40 wt % Teflon®; 10 wt % Pt/C.

## 4. Conclusions

A mathematical model of the electrochemical behaviour of a phosphoric acid fuel cell cathode is proposed. The model results were compared with experimental data: the agreement was found to be satisfactory (less than 20 mV difference), thus confirming the validity of the model.

*Table 2. Base-case values of the model parameters*

| *Parameter* | *Value* | *Reference* |
|---|---|---|
| Electrolyte ionic conductivity | 0.6 $\Omega^{-1}$ $cm^{-1}$ | [9] |
| Exchange current density | $10^{-4}$ mA $cm^{-2}$ | [2] |
| Oxygen solubility–diffusivity product | $6.3 \times 10^{-12}$ mol $cm^{-1}$ $s^{-1}$ | [9] |
| Average agglomerate pore radius | 30 μm | [11] |
| Average agglomerate porosity | 70% | [11] |
| Catalyst utilization | 48% | [11] |
| Catalyst layer thickness | 200 μm | [11] |
| Fraction of Teflon® in the catalyst layer | 40% | [11] |
| Fraction of Pt in the catalyst layer | 10% | [11] |
| Percentage of acid in the catalyst layer | 57% | Eqn 25 here |
| Pt loading in the catalyst layer | 0.5 mg $cm^{-2}$ | [11] |
| Catalyst surface area | 65 $m^2$ $g^{-1}$ | [11] |
| Diffusional layer thickness | 400 μm | [11] |
| Diffusional layer porosity | 65% | [11] |

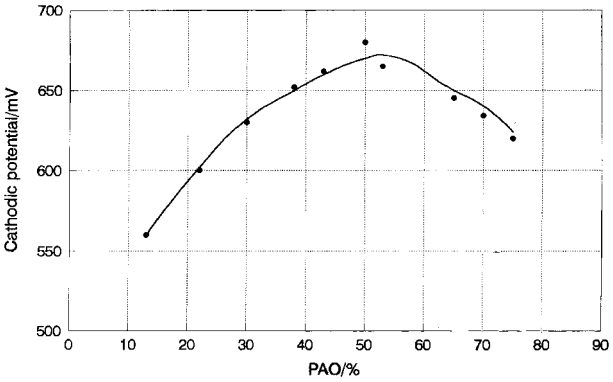


Fig. 7. Experimental (●) and calculated (—) cathodic potential at 200 mA $cm^{-2}$ as a function of the percentage of acid occupying the catalyst layer (*PAO*). Conditions: as in Fig. 3.

A sensitivity study was carried out to evaluate the influence of different parameters on cathodic polarization. The results allowed an optimization of the cathode preparation procedure and an improvement in performance of the fuel cell, whose power increased from 75 to 102 mW $cm^{-2}$.

The present approach, similar to other literature models [15–18], provides a realistic description of the PAFC cathode behaviour based on physico-chemical parameters which are easy to determine.

## References

[1] R. Darby, *Advanced Energy Conversion* **5** (1965) 43.
[2] J. Giner and C. Hunter, *J. Electrochem. Soc.* **116**(2) (1969) 1124.
[3] H. C. Maru, C. Chi, D. Patel and D. Burns, Proceedings of the 13th International Society Energy Conversion Engineering Conference, San Diego, Vol. 1 (1978), p. 723.
[4] C. Y. Yuh and J. R. Selman, *J. Electrochem. Soc.* **131**(9) (1984) 2062.
[5] C. Y. Lu and T. M. Maloney, 'Mathematical Modeling of Solid Oxide Fuel Cells', Report DOE/NASA/0017-5, CR-182188 (1988).
[6] T. E. Springer, T. A. Zawodzinski and S. Gottesfeld, *J. Electrochem. Soc.* **138**(8) (1991) 2334.
[7] G. L. Lee, J. R. Selman and L. Plomp, 'Symposium on Modeling of Batteries and Fuel Cells', Vol. 91-10, The Electrochemical Society, Pennington, NJ (1991), p. 140.
[8] M. Mulder, 'Basic Principles of Membrane Technology' (Kluwer Academic, Dordrecht, 1992).
[9] J. Vossen, 'Models for Porous Electrodes', Delft University of Technology Report, Faculty of Chemical Engineering and Materials Science, Delft (1988).
[10] H. R. Kunz and G. A. Gruver, *J. Electrochem. Soc.* **122**(10) (1975) 1279.
[11] E. Passalacqua and G. Maggio, 'Mathematical Model for Phosphoric Acid Fuel Cell Cathodes', CNR-TAE Report 2/93 (Apr. 1993).
[12] S. Motoo, M. Watanabe and N. Furuya, *J. Electroanal. Chem.* **160** (1984) 351.
[13] D. S. Chan and C. C. Wan, *J. Power Sources* **50** (1994) 261.
[14] J. A. S. Bett, H. R. Kunz, S. W. Smith and L. L. Van Dine, 'Investigation of Alloy Catalysts and Redox Catalysts for Phosphoric Acid Electrochemical Systems', prepared by International Fuel Cells for the Los Alamos National Laboratory under contract 9-X13-D6271-1 (1985).
[15] P. Björnbom, *Electrochim. Acta* **32**(1) (1987) 115.
[16] M. B. Cutlip, S. C. Yang and P. Stonehart, *Electrochim. Acta* **36**(3/4) (1991) 547.
[17] D. M. Bernardi and M. W. Verbrugge, *AIChE J.* **37**(8) (1991) 1151.
[18] J. Kim, S-M. Lee, S. Srinivasan and C. E. Chamberlain, *J. Electrochem. Soc.* **142**(8) (1995) 2670.